Sustainable Food Technology

ROYAL SOCIETY OF CHEMISTRY

PAPER

View Article Online
View Journal | View Issue



Cite this: *Sustainable Food Technol.*, 2024, **2**, 152

# Formation of nanoporous aerogels from defatted rice bran *via* supercritical carbon dioxide drying

Sumanjot Kaur,[a] Jingyi Chen [b] and Ali Ubeyitogullari *[ac]

Rice bran (~8–10% of the total rice weight), generated in large quantities during rice processing, is an underutilized rice processing byproduct. The objective of this study was to upcycle defatted rice bran into starch and protein-based nanoporous aerogels using supercritical carbon dioxide (SC-$CO_2$) drying. Specifically, crude starch-1, crude starch-2, and protein aerogels were prepared at three different concentrations of 10, 15, and 20% (w/w). The generated aerogels were characterized for their morphology, crystallinity, chemical interactions, textural properties, solubility, and thermal stability. The aerogels (15%, w/w) prepared from rice bran crude starch and protein formed a three-dimensional interconnected open porous structure. At this concentration, protein aerogels revealed the highest surface area of 25.3 $m^2\ g^{-1}$, a pore size of 22 nm, and a pore volume of 0.13 $cm^3\ g^{-1}$, whereas crude starch-1 and crude starch-2 aerogels had surface areas of 19.7 and 21.3 $m^2\ g^{-1}$, pore sizes of 22 and 18 nm, and pore volumes of 0.10 and 0.09 $cm^3\ g^{-1}$, respectively. All the aerogels exhibited densities lower than 0.3 g $cm^{-3}$ with porosities higher than 82%. Overall, this study generated high-value starch and protein-based aerogels that can be used for developing functional foods to deliver bioactive compounds, thereby adding value to the underutilized defatted rice bran.

Received 10th May 2023
Accepted 21st October 2023

DOI: 10.1039/d3fb00069a

rsc.li/susfoodtech



### Sustainability spotlight

Rice bran, generated in large quantities during rice processing, is an underutilized rice processing byproduct. To date, rice bran has been only commercialized for oil production, and the rest is used as animal feed, feedstock, and boiler fuel, and in biohydrogen production. The objective of this study was to upcycle defatted rice bran into starch and protein-based nanoporous aerogels using supercritical carbon dioxide drying. This study generated high-value starch and protein-based aerogels that can be used for developing functional foods to deliver bioactive compounds, thereby adding value to the underutilized defatted rice bran. Thus, this study advances the UN's Sustainable Development Goals (SDG) 2: end hunger, achieve food security and improved nutrition and promote sustainable agriculture (*i.e.*, SDG 2.4), and 12: ensure sustainable consumption and production patterns (*i.e.*, SDG 12.3).

## 1. Introduction

Growing global demand for rice consumption increased the rice processing byproduct production in the same proportion. Rice bran (~8–10% of the total grain weight) is an underutilized rice processing byproduct, of which more than 50 MT is produced annually.[1] To date, rice bran has been only commercialized for oil production, and the rest is used as animal feed, feedstock, and boiler fuel, and in biohydrogen production.[2,3] Defatted rice bran, a great source of high-value starch (30–40%) and protein (13–14%), has recently gained a lot of attention due to its high-value essential amino acid content, gluten-free nature and potential health benefits, including antioxidant activities, and antiallergic and anticancer properties.[4]

Starch and proteins from defatted rice bran are food-grade, low-cost, biodegradable, and renewable materials with high potential for food applications. The rice bran starch is composed of amylose and amylopectin, and proteins are composed of albumin, globulin, glutelin, and prolamin.[1] Additionally, rice bran is a rich source of fiber that has several potential health benefits, including improving digestion, reducing cholesterol levels, and maintaining overall gut health.[5] Even though there have been recent efforts to use rice bran in food applications (*e.g.*, bakery products) in addition to its use as animal feed, they are still minimal.[6] Owing to its high nutritional value, defatted rice bran is a great source to produce food-grade bio-based aerogels to convert rice processing byproducts into high-value materials and contribute to enhancing the sustainability of rice production.

Production of bio-based aerogels has increased in the past few decades due to their biodegradability, high surface area, high porosity, low thermal conductivity, low relative density,

[a]*Department of Food Science, University of Arkansas, Fayetteville, N205, 2650 N. Young Ave, AR 72704, USA. E-mail: uali@uark.edu; Tel: +1 (479)-575-3183*
[b]*Department of Chemistry and Biochemistry, University of Arkansas, Fayetteville, AR 72701, USA*
[c]*Department of Biological and Agricultural Engineering, University of Arkansas, Fayetteville, AR 72701, USA*

and open porous three-dimensional structure for numerous applications, such as bioactive compound/drug delivery, tissue engineering, disease diagnosis, and antibacterial materials.[7–10] Aerogels are generated upon drying of gels with a network structure *via* SC-$CO_2$. SC-$CO_2$ eliminates surface tension and capillary forces during drying, resulting in high-surface-area, nanoporous materials. Compared to SC-$CO_2$ drying, both air and freeze-drying lead to shrinkage during drying, creating materials with low surface areas.[11–13] For example, SC-$CO_2$ drying of high amylose corn starch gels resulted in a surface area of 175 $m^2\ g^{-1}$, while freeze-drying of the same gel produced materials with a very low surface area of less than 1 $m^2\ g^{-1}$.[12] Furthermore, various studies have reported the formation of aerogels from different starches, including wheat,[11] corn,[12,14] and pea.[15] In addition, protein-based aerogels have been generated from canola seed,[16] whey protein,[17] and soy protein.[18] Even though there have been several studies on the generation of aerogels from various starch and protein sources, there is a need for novel, inexpensive sources to create aerogels with potential health benefits. We hypothesized that undervalued defatted rice bran fractions could create high surface area, nanoporous aerogels upon SC-$CO_2$ drying. To the best of our knowledge, there is no report on aerogel formation from defatted rice bran starch and protein. Furthermore, the utilization of rice processing byproducts in the form of aerogels can be an innovative solution to address waste management and sustainability in the rice processing industry.

Therefore, the main objective of this study was to form starch- and protein-based aerogels from defatted rice bran using SC-$CO_2$ drying. Specific objectives were to (i) extract crude starch-1, crude starch-2 with high fiber content, and protein from defatted rice bran and create aerogels from these fractions, and (ii) characterize the produced aerogels for their surface area, pore size, pore volume, density, porosity, emulsifying capacity, morphology, crystallinity, and chemical structure. Considering the low cost and nutritional value of defatted rice bran, the fabricated crude starch-1, crude starch-2, and protein aerogels can be used for the delivery of bioactive compounds/drugs in the food and pharmaceutical industries.

## 2. Materials and methods

### 2.1. Materials

Rice bran was kindly supplied by Riceland Foods (AR, USA). Sodium hydroxide, hydrochloric acid, potassium hydroxide, sodium acetate, and sodium phosphate were purchased from Sigma-Aldrich (MO, USA). Organic solvents, including ethanol, acetone, diethyl ether, and hexane, were purchased from Fisher Scientific (PA, USA), and carbon dioxide (>99.99%) was supplied by Airgas, Inc. (AR, USA). The total starch assays were purchased from Neogen (Lansing, MI).

### 2.2. Defatting rice bran

The defatting of rice bran was performed using hexane according to Ju *et al.*[19] Briefly, 100 g of the sample was mixed with 400 mL of hexane for 4 h, and then the filtered residue was kept for 24 h for drying under a hood at room temperature (23 °C). The extraction was repeated three times.

### 2.3. Protein and crude starch extraction

Protein and crude starch extractions were conducted according to Ju *et al.*[19,20] and Gnanasambandam and Hettiarachchy,[19,20] respectively. In brief, the defatted rice bran sample was mixed with deionized water (1 : 4, w/w), and the pH was adjusted to 9.5 using 1 M NaOH solution. The sample was then centrifuged for 30 min at 10 000*g*. The supernatant was collected for protein extraction, and the residue was prepared for crude starch extraction. The pH of the collected supernatant was adjusted to 4.5 and kept for protein precipitation. The precipitate was centrifuged at 10 000*g* for 30 min. The protein precipitate was washed using deionized water at pH 7.0 and frozen at −80 °C for 24 h before freeze-drying (Labconco, MO, USA).

The spent rice bran obtained after protein extraction was either used as is and called "crude starch-2" or further purified to obtain the starch fraction. The purified starch fraction (hereafter called "crude starch-1") was collected by passing crude starch-2 through a 263-mesh sieve with an opening size of 63 μm.[21] The crude starch-1 fraction was washed using 600 mL of water, 300 mL of ethanol, 300 mL of acetone, and 300 mL of diethyl ether consecutively, where each washing step was repeated twice. Finally, the extracts of crude starch-1 and crude starch-2 were collected by centrifugation and dried overnight under a hood for 24 h at room temperature (23 °C). After complete drying, the samples were stored at −4 °C until further use.

### 2.4. Compositional analysis

The moisture content was determined according to the AACC 2000 method.[22] The nitrogen content was determined according to AOAC 968.06-1969 and converted into crude protein content by using a conversion factor of 6.25.[23] The ash content was determined according to AOAC 923.03.[24] The starch content was quantified following the method of AOAC 996.11.[25]

### 2.5. Aerogel formation

The formation of aerogels involved three main steps: hydrogel formation, solvent exchange, and SC-$CO_2$ drying, as depicted in Fig. 1.

**2.5.1. Hydrogel formation.** The crude starch-1 and crude starch-2 hydrogels were prepared according to Ahmadzadeh and Ubeyitogullari.[26] In brief, different concentrations (10, 15, and 20%, w/w) of crude starch-1 and crude starch-2 suspensions were prepared, and heated to 95 °C and kept at that temperature for 25 min under continuous stirring (600 rpm) with a magnetic stirrer. The formed starch-based gels, upon cooling, were kept at 4 °C for 48 h for retrogradation. Similarly, protein hydrogels were prepared at different concentrations (10, 15, and 20%, w/w) following the method of Dey *et al.*[27] First, protein suspensions were homogenized using a probe ultrasound processor (Cole-Parmer Instruments, IL, USA). The probe ultrasound processor was operated using the following settings: time: 5 min, temperature: 20 °C, pulse rate: 5 s on, 1 s off. After the

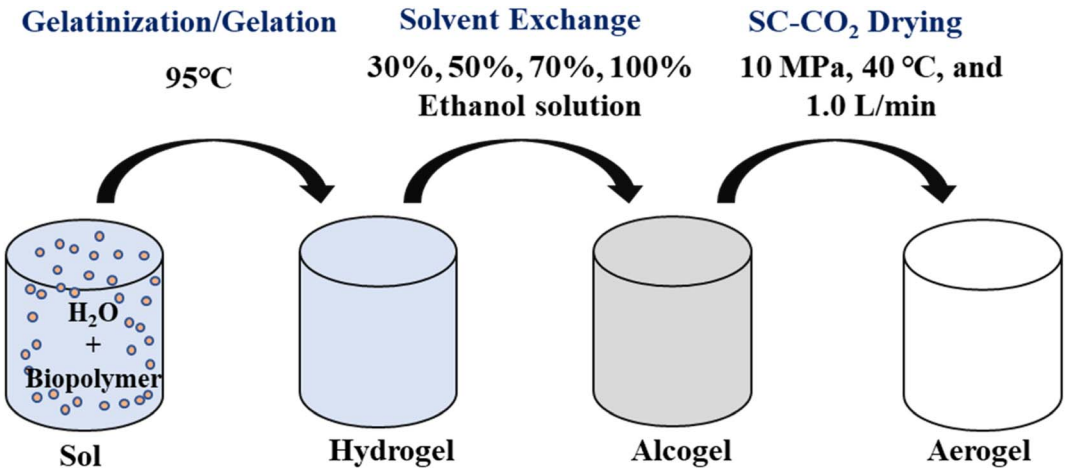


Fig. 1 The main steps involved in aerogel formation.

treatment with ultrasound, the protein solutions were heated to 85 °C for 20 min in a water bath (Boekel, PA, USA). Finally, the formed protein hydrogels were kept at 4 °C for 48 h before the solvent exchange step. All the samples were covered with aluminum foil to minimize water loss during heating.

**2.5.2. Solvent exchange.** The hydrogels were cut into small pieces 1–2 cm in length, and solvent exchange was performed in five steps.[11] In short, the samples were immersed in different ethanol concentrations in water (30, 50, 70, and 100%, v/v) for a 1 h period each, and next, they were kept in 100% ethanol for 24 h to form alcogels.

**2.5.3. SC-$CO_2$ drying.** The produced alcogels were dried using SC-$CO_2$ according to the conditions optimized by Ubeyitogullari and Ciftci.[11] The optimized drying conditions, *i.e.*, pressure (10 MPa), temperature (40 °C), and $CO_2$ flow rate (1.0 L $min^{-1}$, measured under ambient conditions of 23 °C and 0.1 MPa), were followed during SC-$CO_2$ drying in a lab-scale dryer (SFT-120, Supercritical Fluid Technologies Inc., DE, USA). First, the sample was loaded into a ~50 mL basket with two stainless steel frits placed at the bottom of it to make sure that the sample was covered with ethanol before drying, and $CO_2$ flow was enabled through the basket. The basket was placed in a 100 mL high-pressure vessel with glass wool placed at both ends of the vessel. The vessel and micrometering valve temperatures were set to 40 and 80 °C, respectively. The micrometering valve was heated to prevent freezing due to the Joule–Thomson effect. After the set temperatures were attained, the system was pressurized to 10 MPa. SC-$CO_2$ drying continued for 4 h with a $CO_2$

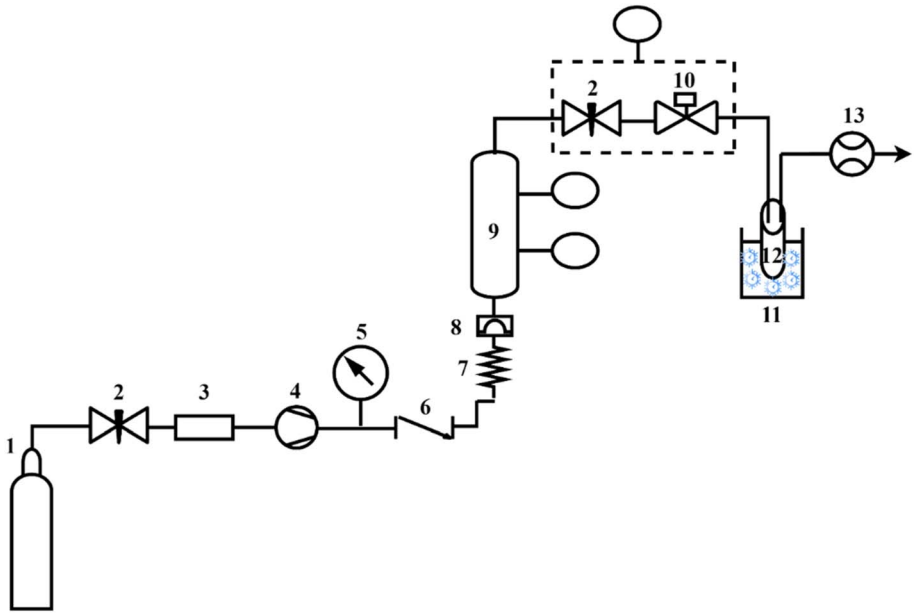


Fig. 2 Schematic diagram of the SC-$CO_2$ system used for drying. Tags refer to: (1) $CO_2$ cylinder; (2) needle valve; (3) pre-chiller; (4) high-pressure pump for $CO_2$; (5) pressure gauge; (6) check valve; (7) preheater; (8) rupture disc; (9) high-pressure vessel; (10) micrometering valve; (11) cold trap; (12) vial; and (13) flow meter.

flow rate of 1.0 L $min^{-1}$ (measured under ambient conditions of 23 °C and 0.1 MPa). After 4 h of drying, the system was depressurized at the same $CO_2$ flow rate. Finally, the aerogels were collected and stored at room temperature (23 °C) in airtight containers (Fig. 2).

### 2.6. Aerogel characterization

**2.6.1. Morphology.** The morphology of the samples was determined using a scanning electron microscope (SEM, FEI NovaNanoLab200 Dual-Beam system, FEI company, OR, USA). The samples were coated with a gold layer using a sputter-coater (EMITECH SC7620 Sputter Coater, MA, USA) prior to imaging. The SEM images were taken using the vacuum mode at 5 mm working distance, 15 kV, and 15 mA.

**2.6.2. Surface area, pore size, pore volume, porosity, and shrinkage.** The aerogels were analyzed for Brunauer–Emmett–Teller (BET) surface area and Barrett–Joyner–Halenda (BJH) pore size and pore volume using low-temperature nitrogen adsorption–desorption analysis (ASAP 2460, Micromeritics Instrument Corporation, GA, USA). In brief, 0.06–0.3 g samples were prepared by cutting aerogels into small pieces and degassed at 115 °C for 4 h.[12] Nitrogen sorption experiments were carried out at −196 °C. The specific surface area was determined by multipoint BET adsorption characteristics at a relative pressure ($p/p_0$; equilibrium pressure of nitrogen at the sample surface/saturation pressure of nitrogen) between 0.05 and 0.3. The BJH pore size and volume were determined at relative pressures ($p/p_0$) greater than 0.35. Additionally, the porosities of crude starch and protein aerogels were calculated using the following equation (eqn (1)).[28]

$$\text{porosity}(\%) = \left(1 - \frac{\text{bulk density}}{\text{true density}}\right) \times 100 \quad (1)$$

The bulk density was measured by using the ratio of weight to volume, and the true density was determined using a gas pycnometer AccuPyc II 1340 (Micromeritics, GA, USA). The true density measurement was conducted at 25 °C using a cell with 10 $cm^3$ volume, where both cycle and purge fill pressures were fixed at 19.5 psig.

The volumetric shrinkage of the aerogels during solvent exchange and drying was calculated using the following equation:

$$\text{volumetric shrinkage}(\%) = \left(1 - \frac{V_a}{V_b}\right) \times 100 \quad (2)$$

where $V_a$ is the aerogel volume after drying and $V_b$ is the volume of the hydrogel before solvent exchange.[26]

**2.6.3. Crystallinity.** The XRD patterns were recorded using an X-ray diffractometer (PW3040X'PertMRD, Philips, Almelo, Netherlands). The powdered aerogel samples were scanned at 45 kV and 40 mA in a range of 5–40° with a step size of 0.02° $s^{-1}$.

**2.6.4. Chemical interactions.** Fourier transform infrared spectroscopy (FTIR, IRAffinity-IS Fourier transform infrared spectrometer, SHIMADZU Corp., Kyoto, Japan) was used to survey the chemical interactions in the samples. The FTIR spectrometer was equipped with a Quest attenuated total reflectance (ATR) accessory (Specac Company, Orpington, UK). The samples were scanned between 400 and 4000 $cm^{-1}$ wavenumbers at a resolution of 4 cm with 64 scans.[29]

**2.6.5. Thermal stability.** The thermogravimetric analysis (TGA) of the samples was conducted using a TA Q50 (TA Instruments, DE, USA) according to Wang *et al.*[30] Approximately 10 mg of the sample was loaded into an aluminum pan using a microbalance. The sample was first kept at 30 °C for 10 min and then heated to 600 °C at a rate of 10 °C $min^{-1}$ under a flow of nitrogen at 20 mL $min^{-1}$.

**2.6.6. Water solubility.** The water solubility of the extracts and aerogels was determined according to Ubeyitogullari and Ciftci.[11] In short, 0.5 g of the sample was mixed with 50 mL of distilled water. The mixture was then heated in a water bath (Boekel, PA, USA) at 60 °C for 10 min. Then, the solution was centrifuged at 670 *g* for 20 min (Heraeus multifuge XIR, Germany). A known volume of supernatant was dried at 103 °C until a constant weight was reached. The solubility was calculated according to the following equation (eqn (3)):

$$\text{Solubility}(\%, \text{w/w}) = \frac{\text{Weight of the dissolved solids in supernatant}}{\text{Weight of the sample}} \times 100 \quad (3)$$

### 2.7. Statistical analysis

The statistical analysis was performed using ANOVA and Tukey's test at a 5% significance level with statistical software JMP Pro 16.0 (SAS Institute, NC, USA). The experiments were conducted in triplicate, and the results were expressed as the mean ± standard deviation.

## 3. Results and discussion

### 3.1. Composition of rice bran

The composition of rice bran is illustrated in Table 1. The rice bran used for aerogel production contained 31.7% starch, 13.8% protein, 12.7% oil, and 14.6% ash, which were in agreement with the previously published composition data.[31–33] The moisture content of the rice bran (2.5%, w/w) was relatively low compared to that in previous reports (8–11%, w/w).[34] Vaitkeviciene *et al.* reported a resistant starch content of 11.5% in rice bran.[35] According to the literature, the amylose content in

Table 1 The composition of rice bran[a]

| Rice bran | Composition (%, w/w) |
|---|---|
| Protein | 13.84 ± 0.11[b] |
| Starch | 31.66 ± 1.67[a] |
| Oil | 12.71 ± 0.53[b] |
| Moisture | 2.52 ± 0.15[c] |
| Ash | 14.60 ± 0.42[b] |

[a] Means that do not share a common letter are significantly different ($p < 0.05$).

rice bran starch is quite low (0.49–6%), and peptide fractionization from defatted rice bran showed 12.5% albumin, 13.9% globulin, 70.8% glutelin and 2.9% prolamin.[36–38] As discussed by Kalpanadevi *et al.* the differences in the composition data could be due to many reasons, including different varieties of rice, environmental factors, and milling conditions.[39]

### 3.2. Fabrication of the aerogels

In this study, crude starch-1, crude starch-2, and protein hydrogels were fabricated using different concentrations (10, 15, and 20%) (Fig. 3). The starch contents of the crude starch-1 and crude starch-2 fractions were 66.1% and 51.4% (dry basis), respectively, while the protein fraction contained 60.0% (dry basis) proteins. The results showed that the minimum hydrogel concentration required to maintain the shape was 15%. However, below this concentration (10%), it was difficult to maintain the shape, and an increase in concentration to 20% led to a denser structure with higher viscosity. The reason for not being able to form strong gels with 10% crude starch-1 and -2 could be due to their low starch concentrations (66.1% and 51.4%, respectively). Forming hydrogels from the collected fractions (*i.e.*, crude starch-1 and-2, and protein) without extensive purification steps could reduce the cost of the materials used for aerogel fabrication. Due to the higher solubility of ethanol in SC-$CO_2$, the hydrogels were introduced to different ethanol concentration solutions to replace the water in the matrix with ethanol.[40] The formed alcogels were dried using SC-$CO_2$ drying, preserving the porous structure by reducing the capillary stress on the matrix and preventing shrinkage.

### 3.3. Morphology

The three-dimensional open porous network structure was not observed in the crude starch-1 (Fig. 4a1 and A1), crude starch-2 (Fig. 4b1 and B1), and protein (Fig. 4c1 and C1) extracts. Additionally, the presence of globules in the crude starch-1 and crude starch-2 extracts indicated the presence of calcium carbonate in the samples.[41] This was also confirmed by the high crystalline peaks observed in the XRD patterns (Fig. 5). Since calcium carbonate is not soluble in water, it was collected in crude starch-1 and crude starch-2 fractions, and was not present in the protein fraction after extraction. Calcium carbonate is commonly used to enhance the milling of rice at the industrial scale.[42]

The crude starch-1, crude starch-2, and protein aerogels exhibit a three-dimensional open porous network with interconnected fibrils, which became denser as concentration increased from 10 to 20% (Fig. 4). The SEM images of protein aerogels at high magnifications (Fig. 4C2–4) revealed a more

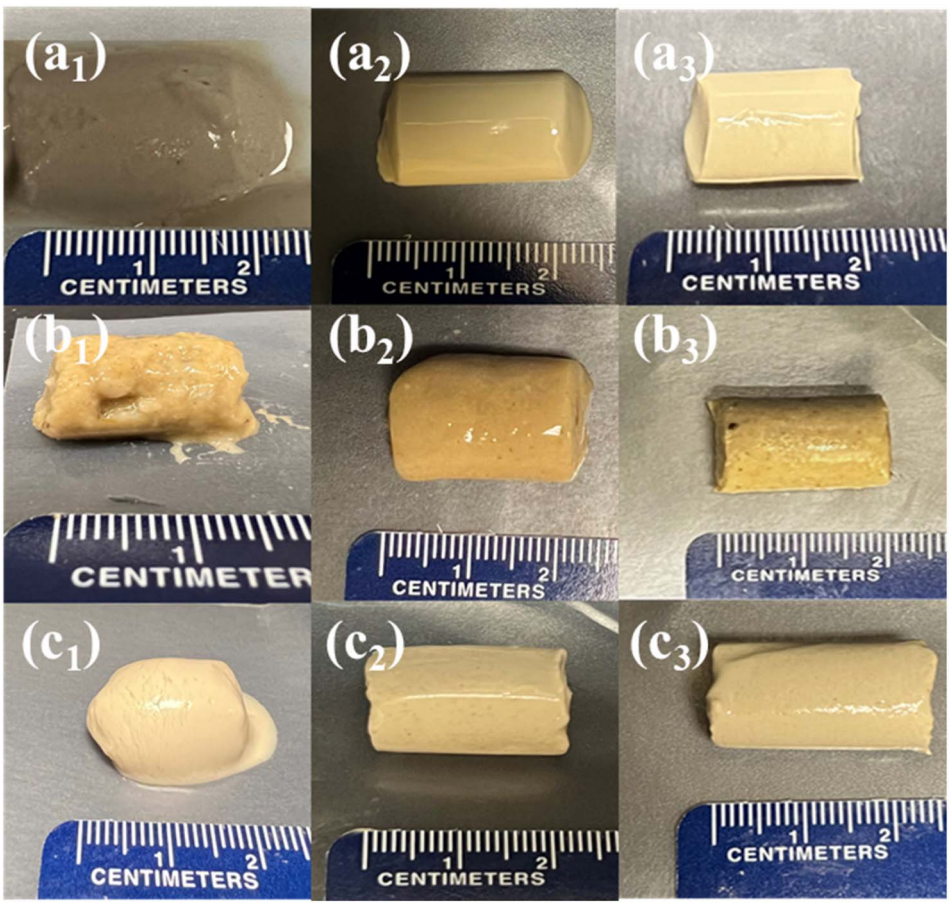


Fig. 3 Pictures of crude starch-1, crude starch-2, and protein hydrogels at 10 ($a_1$–$a_3$), 15 ($b_1$–$b_3$), and 20% ($c_1$–$c_3$), respectively.

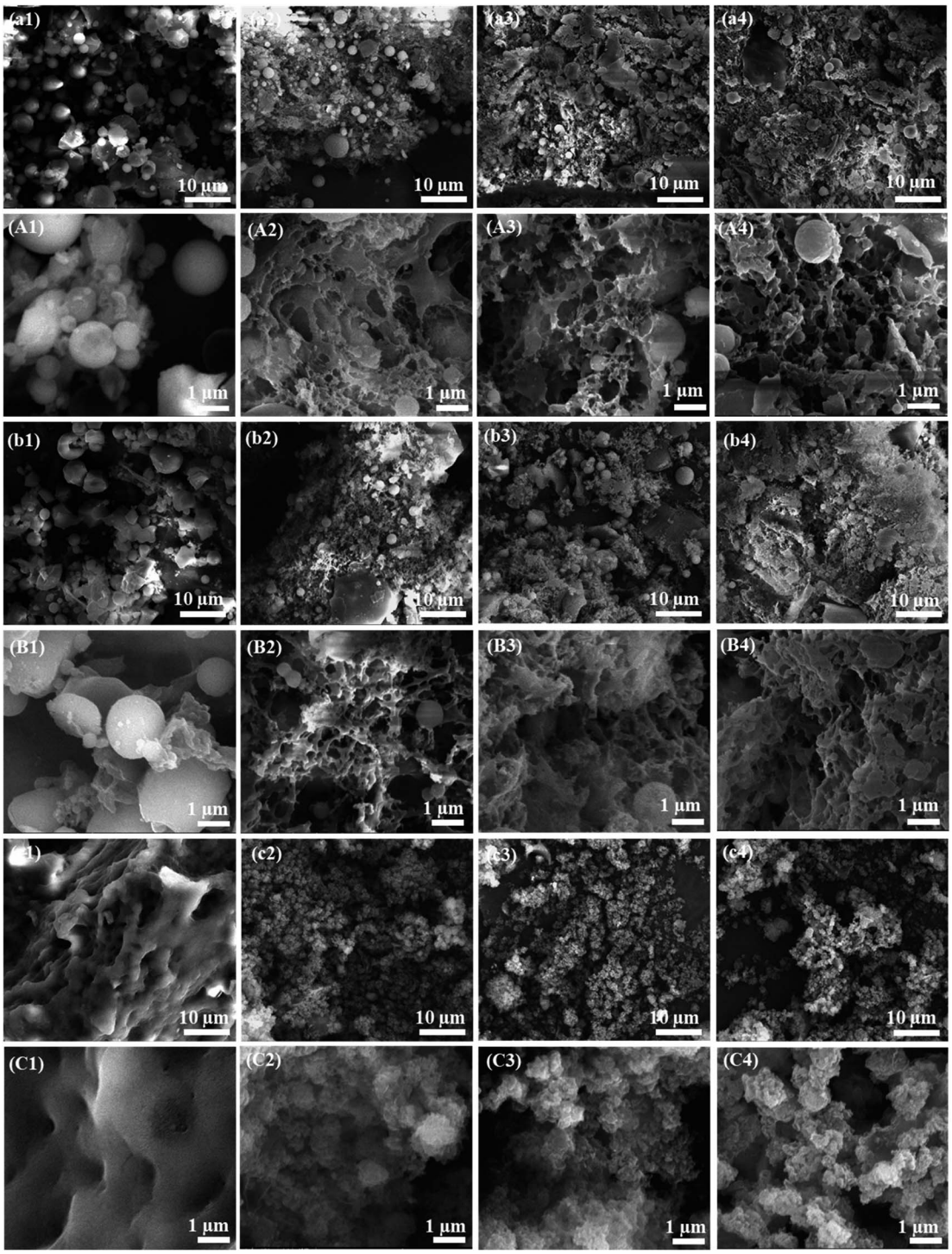


Fig. 4 The SEM images of extracts: (a1 and A1) crude starch-1, (b1 and B1) crude starch-2, and (c1 and C1) protein; and aerogels with different concentrations: 10% (a2 and A2) crude starch-1, (b2 and B2) crude starch-2, and (c2 and C2) protein; 15% (a3 and A3) crude starch-1, (b3 and B3) crude starch-2, and (c3 and C3) protein, and 20% (a4 and A4) crude starch-1, (b4 and B4) crude starch-2, and (c4 and C4) protein at low and high magnifications, respectively.

globular structure due to strong repulsive forces of protein molecules.[16] The presence of fiber in the crude starch-2 aerogel revealed a significant difference in the macrostructure as compared to that of the crude starch-1 aerogel. The findings were further justified using surface area, pore size, density, and porosity, as discussed in Table 2. Likewise, aerogels from wheat, corn, and pea starches showed a similar three-dimensional open porous structure.[11,15] FitzPatrick *et al.* revealed a porous network formed using canola seed protein aerogels.[16] Therefore, gels with 15% concentration were further optimized based

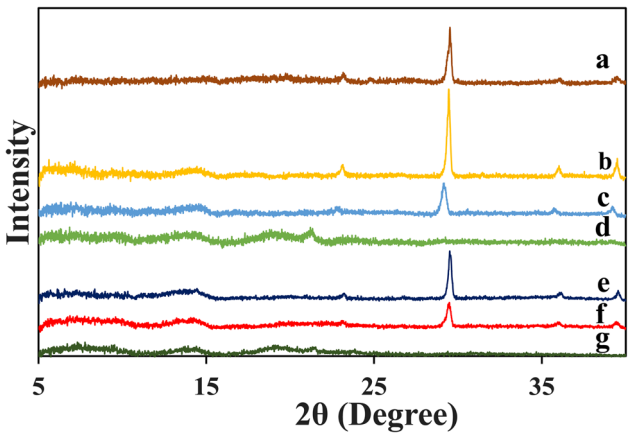


Fig. 5 XRD patterns of (a) rice bran, (b) crude starch-1, (c) crude starch-2, and (d) protein extracts, and aerogels formed using 15% (w/w) (e) crude starch-1, (f) crude starch-2, and (g) protein.

on their ability to maintain the gel structures better than the 10% gels and their lower densities compared to the 20% gels.

### 3.4. Surface area, pore size, pore volume, porosity, and shrinkage

As discussed above, 15% (w/w) crude starch-1, crude starch-2, and protein aerogels were used for further characterization. BET surface area, BJH pore size and pore volume of these aerogels are reported in Table 2. Among the aerogels, the protein aerogels showed the highest surface area of $25.25 \pm 0.83$ $m^2$ $g^{-1}$ and pore volume of $0.13 \pm 0.01$ $cm^3$ $g^{-1}$. However, crude starch-1 showed the lowest surface area ($19.72 \pm 0.19$ $m^2$ $g^{-1}$), and lowest pore volume ($0.09 \pm 0.00$ $cm^3$ $g^{-1}$). The textural properties depend on the starch type, amylose content, and amylose/amylopectin ratio. Ubeyitogullari and Ciftci generated wheat starch (15%) aerogels with a higher surface area (~60 $m^2$ $g^{-1}$), which might be due to the different approach followed for hydrogel formation (*e.g.*, gelatinization at 120 °C), and the use of a different type of starch.[11,43] Wang *et al.* reported 17.3 $m^2$ $g^{-1}$ surface area in a corn starch aerogel.[43] In a previous study, the egg white protein aerogel's surface area highly depended on the pH, where the lowest surface area (16 $m^2$ $g^{-1}$) was reported at pH values closer to the isoelectric point.[44]

The surface areas of the aerogels obtained in this study were lower than the ones reported in the literature, which was mostly due to the differences in the gel formation step (magnetic stirrer *vs.* high-shear mixer), and type/source of the materials (*i.e.*, rice bran starch and protein). For example, gel formation with a high-shear mixer resulted in a more porous structure compared to that with a magnetic stirrer in our previous study.[12] In addition, the purities of the starch and protein extracts were relatively low as described in Section 3.2, which may have also negatively affected the gelatinization/gelation in forming a porous network.

The results indicated that crude starch-1 and protein aerogels have the highest densities of 0.25 and 0.26 g $cm^{-3}$, respectively, compared to the crude starch-2 aerogel (0.22 g $cm^{-3}$) ($p < 0.05$). Additionally, the crude starch-1 (86%) and crude starch-2 (87%) aerogels showed higher porosities than protein aerogels (82%). Similar densities were previously reported for aerogels from canola protein (~0.2 g $cm^{-3}$), whey protein (0.22 g $cm^{-3}$), and egg white (~0.3 g $cm^{-3}$).[16,17,44] Likewise, the densities of starch aerogels from wheat (0.23 g $cm^{-3}$) and maize (0.24 g $cm^{-3}$) were comparable to the data reported here for rice bran starch aerogels.[15,45] The crude starch-1 and protein revealed higher shrinkages of 47 and 58%, respectively, compared to crude starch-2 (26%). The reduced shrinkage of crude starch-2 could be due to its higher fiber content, which might have supported the structure during solvent exchange and drying. This finding also supports the lower surface area of crude starch-1 in comparison with that of crude starch-2.

### 3.5. Crystallinity

XRD patterns of the extracts and aerogels (prepared with 15% concentration) are depicted in Fig. 5. The results indicated the presence of calcium carbonate in the rice bran sample, as evidenced by four major diffraction peaks at $2\theta = 23.25°$, 29.51°, 35.98°, and 39.44°.[46] Similarly, calcium carbonate crystalline peaks were highly visible in the rice bran crude starch-1 and crude starch-2 extract and aerogels, which supported the data obtained by SEM (Fig. 4). In addition, the extracted crude starch-1 showed high-intensity crystalline peaks in the $2\theta$ range of 15° to 23°, which corresponded to A-type and B-type patterns.[47–49] Additionally, the protein samples showed diffraction peaks at $2\theta = 7.24°$, 9.64°, 13.78°, 14.38°, 18.88°, 21.2°, and 23.89°. Lu *et al.* revealed a high crystallinity of starch due to the formation of complexes between starch and hydrophobic peptides.[48] However, gelatinization caused a transformation of A-type and B-type crystalline peaks, resulting in a decrease in the degree of crystallinity.[11] A similar deformation of crystalline peaks was observed in wheat starch and corn starch aerogels.[11,50] Therefore, the reduced crystallinity observed in aerogels was mainly due to structural changes that occurred during gelatinization/gelation and retrogradation. These findings are

Table 2 Textural properties of crude starch-1, crude starch-2, and protein aerogels[a]

| Samples | Surface area ($m^2$ $g^{-1}$) | Pore size (nm) | Pore volume ($cm^3$ $g^{-1}$) | Density (g $cm^{-3}$) | Porosity (%) | Shrinkage (%) |
|---|---|---|---|---|---|---|
| Crude starch-1 | $19.72 \pm 0.19^c$ | $21.68 \pm 1.37^a$ | $0.103 \pm 0.001^b$ | $0.25 \pm 0.01^a$ | $86.43 \pm 0.77^a$ | $47.31 \pm 2.72^b$ |
| Crude starch-2 | $21.26 \pm 0.89^b$ | $18.01 \pm 0.75^b$ | $0.094 \pm 0.001^c$ | $0.22 \pm 0.01^b$ | $87.09 \pm 0.39^a$ | $26.17 \pm 2.33^c$ |
| Protein | $25.25 \pm 0.83^a$ | $21.56 \pm 2.12^a$ | $0.130 \pm 0.001^a$ | $0.26 \pm 0.01^a$ | $81.80 \pm 0.16^b$ | $57.62 \pm 1.38^a$ |

[a] Means in the same column that do not share a common letter are significantly different ($p < 0.05$).

consistent with the previously reported studies related to the formation of starch and protein aerogels.[26,51]

### 3.6. Chemical interactions

The functional groups of extracts and aerogels (15% concentration) were determined using ATR-FTIR (Fig. 6). The characteristic peaks at 1240 $cm^{-1}$ and 1255 $cm^{-1}$ revealed the strong C-N amide bonding, while the peak at 1720 $cm^{-1}$ corresponded to the strong C=O bonding (Fig. 6a–c). Additionally, the peaks at 1060 $cm^{-1}$ and 1120 $cm^{-1}$ indicated strong bonding of C–O stretching in both extract and aerogels. Furthermore, the region at around 1200–1400 $cm^{-1}$ in the FTIR spectrum of the protein extract (Fig. 6c) contributed strongly towards –OH deformation. Also, a strong contribution of aromatic bands at around 900–1250 $cm^{-1}$ was observed in crude starch and protein extracts (Fig. 6a–c). For crude starch-1 and crude starch-2 extracts, C–H alkanes were observed at 2925 $cm^{-1}$.[52] The peaks at 1047 and 1022 $cm^{-1}$ indicate the crystalline and amorphous region in crude starch-1, and the peak ratio of 1047 $cm^{-1}$/1022 $cm^{-1}$ indicates short-range molecular order where a lower ratio was observed in the aerogels after the gelatinization of native starch. This decrease in the 1047/1022 $cm^{-1}$ ratio indicated a decrease in the order degree of the double helical structure.[53] The N–H bond peaks at 1180 $cm^{-1}$ in Fig. 6a and b justified the presence of some proteins in crude starch extracts. Moreover, the findings showed a more ordered short-range structure formation after gelatinization and shifting of peaks in crude starch to 3325 $cm^{-1}$, indicating stronger hydrogen bonding interactions between protein and starch. Lu *et al.* revealed absorption peak shifting to 3389–3306 $cm^{-1}$, indicating the strong interaction between rice protein and starch by hydrogen bonding during their co-gelatinization.[48]

### 3.7. Thermal stability

The thermal stabilities of 15% (w/w) crude starch-1, crude starch-2, and protein aerogels are shown in Fig. 7. The first weight loss was observed in the range of 21–120 °C for protein, crude starch-1, and crude starch-2 aerogels due to moisture loss. Major thermal degradation occurred at 295 °C for all the samples. While crude starch-1 and crude starch-2 aerogels were degraded in the range of 225–350 °C, the protein aerogel showed a wider range of 200–420 °C. At 295 °C, the percentage losses in weight were 42, 48, and 53% for crude starch-1, crude starch-2, and protein aerogels, respectively. After the weight loss, the remaining corresponds to the final char and ash content, resulting in 33% for crude starch-1, 24% for crude starch-2, 26% for protein aerogels, which are comparable to the values (~22%) reported for rice bran.[54] A similar weight loss of 45% in rice bran starch was reported by Fabian *et al.* at 302 °C, and Hasanvand and Rafe reported 62% weight loss in the rice bran protein at 316 °C.[37,55] Overall, the developed aerogels' ability to maintain stability at high temperatures can broaden their potential applications where thermal treatment/processing is required.

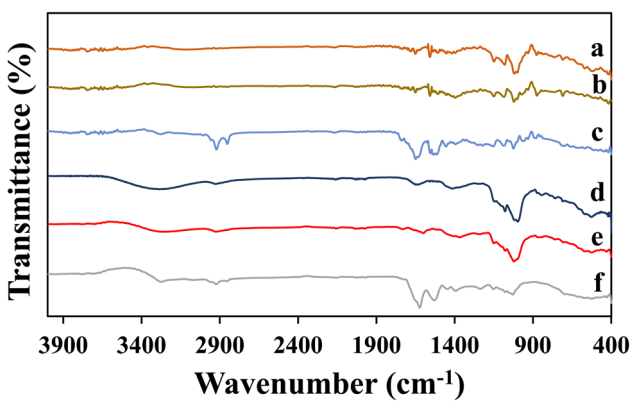


Fig. 6 ATR-FTIR spectra of (a) crude starch-1, (b) crude starch-2, and (c) protein extracts from defatted rice bran, and aerogels formed using 15% (w/w) (d) crude starch-1, (e) crude starch-2, and (f) protein.

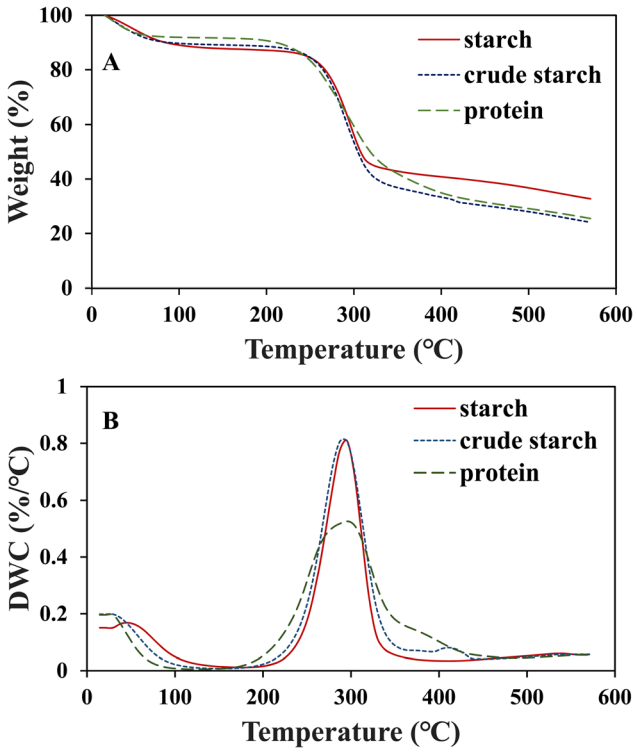


Fig. 7 Thermogravimetric analysis (A) weight loss (%) and (B) derivative weight loss (%) per °C temperature of 15% crude starch-1, crude starch-2, and protein aerogels at a heating rate of 10°C $min^{-1}$ and a nitrogen flow of 20 mL $min^{-1}$.

### 3.8. Water solubility

The water solubilities of crude starch-1, crude starch-2, and protein extracts and aerogels are depicted in Fig. 8. The crude starch-1 (57.47 ± 1.13%) and crude starch-2 (68.21 ± 6.22%) aerogels exhibited significantly higher solubilities in water as compared to their extracts (19.74 ± 2.71% for crude starch-1 and 15.53 ± 0.99% for crude starch 2) ($p < 0.05$), indicating an increase in the amorphous part in the aerogels (Fig. 5).[56] Similarly, the solubility of proteins increased from 16 to 20% after the formation of aerogels. The increase in water solubility after

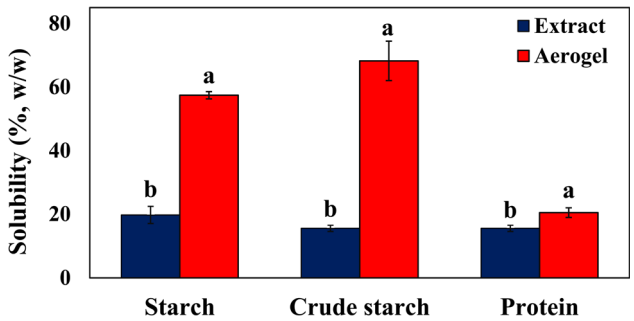


Fig. 8 Water solubility of crude starch-1, crude starch-2, and protein extracts and their aerogels prepared at 15% concentration. Error bars indicate the standard deviation. Means in the same group (*i.e.*, crude starch-1, crude starch-2, and protein) that do not share a common letter are significantly different ($p < 0.05$).

forming the aerogels was mainly related to the gelatinization/gelation steps during aerogel formation, which resulted in reduced crystallinity.[51] The amorphous structure has higher solubility due to its higher free energy.[56] The hydrogen bonding interactions in Fig. 6 also justify the increases in the solubilities of aerogels. Previously, the solubility of rice bran was reported to be from 7.3–8% by Bhosale and Vijayalakshmi.[57] Fabian *et al.* observed an increase in the solubility of starch from 8 to 15% as the temperature increases from 70 to 90 °C due to the leaching of branched molecules into linear molecules.[37,58] Tang *et al.* observed that the solubility of rice bran protein is lower (~10%) closer to the isoelectric point; however, as the pH increases from pH 6 to pH 12, the protein solubility increases to 66%.[59]

## 4. Conclusions

This study illustrated the results of compositional, textural, and morphological analyses of defatted rice bran for aerogel production using a green and sustainable approach based on SC-$CO_2$ drying. The rice bran consisted of starch (32%), protein (14%), oil (13%), ash (15%), and a low moisture content (3%). The SEM images revealed the three-dimensional open porous structure network structure of the aerogels produced using 15% of crude starch-1, crude starch-2, and protein. Compared to crude starch-1 and crude starch-2 aerogels, protein aerogels showed a higher surface area of 25 $m^2\ g^{-1}$, and pore volume of 0.13 $cm^3\ g^{-1}$. Crude starch-1 (0.25 g $cm^{-3}$ and 86%), crude starch-2 (0.22 g $cm^{-3}$ and 87%), and protein (0.26 g $cm^{-3}$ and 82%) aerogels exhibited low densities with high porosities, respectively. The solubilities of crude starch-1, crude starch-2, and protein increased after aerogel formation due to the gelatinization step. Overall, this study reveals a green approach for generating starch and protein aerogels, without extensive separation and purification steps to generate gel formation raw materials from defatted rice bran. The high surface area and porous structure, along with the high fiber content, make the generated aerogels great candidates for delivering bioactive compounds and developing functional foods. This is one of the first studies on the formation of aerogels from defatted rice bran, and therefore, the surface area of the aerogels can be further increased by investigating the gel formation step of aerogel formation.

## Author contributions

Sumanjot Kaur: data curation, formal analysis, methodology, investigation, visualization, writing-original draft; Jingyi Chen: methodology, formal analysis, resources, writing-review & editing; Ali Ubeyitogullari: conceptualization, methodology, investigation, resources, project administration, supervision, writing-review & editing.

## Conflicts of interest

The authors declare no conflict of interest.

## Acknowledgements

This project was supported in part by the USDA National Institute of Food and Agriculture, Multistate Project NC1023, Accession number 1025907, and the University of Arkansas Graduate Student Professional Congress (GPSC) research grant. We also thank Dr Chris Mazzanti for his help with ATR-FTIR measurements.

## References

1 M. Friedman, *J. Agric. Food Chem.*, 2013, **61**, 10626–10641.
2 K. Tomita, S. Machmudah, Wahyudiono, R. Fukuzato, H. Kanda, A. T. Quitain, M. Sasaki and M. Goto, *Sep. Purif. Technol.*, 2014, **125**, 319–325.
3 B. Jha, R. Chandra, V. K. Vijay, P. M. V. Subbarao and A. Isha, *Biomass Bioenergy*, 2020, **140**, 105674.
4 A. A. Mariod, H. A. Adamu, M. Ismail and N. Ismail, *Grasas Aceites*, 2010, **61**, 409–415.
5 T. Jalili, R. E. C. Wildman and D. M. Medeiros, *J. Nutraceuticals Funct. Med. Foods*, 2000, **2**, 19–34.
6 I. Lima, H. Guraya and E. Champagne, *Food/Nahrung*, 2002, **46**, 112–117.
7 E. Malik, S. R. Dennison, F. Harris and D. A. Phoenix, *Pharmaceuticals*, 2016, **9**(4), 67.
8 M. E. El-Naggar, S. I. Othman, A. A. Allam and O. M. Morsy, *Int. J. Biol. Macromol.*, 2020, **145**, 1115–1128.
9 C. A. García-González, M. Alnaief and I. Smirnova, *Carbohydr. Polym.*, 2011, **86**, 1425–1438.
10 M. Tudu and A. Samanta, *Eur. Polym. J.*, 2023, **184**, 111801.
11 A. Ubeyitogullari and O. N. Ciftci, *Carbohydr. Polym.*, 2016, **147**, 125–132.
12 S. Ahmadzadeh and A. Ubeyitogullari, *Carbohydr. Polym.*, 2023, **301**, 120296.
13 M. Guastaferro, E. Reverchon and L. Baldino, *Front. Bioeng. Biotechnol.*, 2021, **9**, 688477.
14 C. A. García-González, M. C. Camino-Rey, M. Alnaief, C. Zetzl and I. Smirnova, *J. Supercrit. Fluids*, 2012, **66**, 297–306.
15 C. A. García-González and I. Smirnova, *J. Supercrit. Fluids*, 2013, **79**, 152–158.

16 S. E. FitzPatrick, S. Deb-Choudhury, S. Ranford and M. P. Staiger, *Eur. Polym. J.*, 2022, **168**, 111126.
17 L. Manzocco, S. Plazzotta, J. Powell, A. de Vries, D. Rousseau and S. Calligaris, *Food Hydrocolloids*, 2022, **122**, 107117.
18 J. C. Arboleda, M. Hughes, L. A. Lucia, J. Laine, K. Ekman and O. J. Rojas, *Cellulose*, 2013, **20**, 2417–2426.
19 Z. Y. Ju, N. S. Hettiarachchy and N. Rath, *J. Food Sci.*, 2001, **66**, 229–232.
20 R. Gnanasambandam and N. S. Hettiarachchy, *J. Food Sci.*, 1995, **60**, 1066–1069.
21 L. Wang and Y.-J. Wang, *Cereal Chem.*, 2001, **78**, 690–692.
22 R. He, Y. Wang, Y. Zou, Z. Wang, C. Ding, Y. Wu and X. Ju, *J. Sci. Food Agric.*, 2020, **100**, 2638–2647.
23 K. X. Zhang, K. Y. Zhang, T. J. Applegate, S. P. Bai, X. M. Ding, J. P. Wang, H. W. Peng, Y. Xuan, Z. W. Su and Q. F. Zeng, *Poult. Sci.*, 2020, **99**, 1001–1009.
24 D. Zhang, L. Wang, B. Tan and W. Zhang, *Int. J. Food Sci. Technol.*, 2020, **55**, 2188–2196.
25 F. Ye, L. Xiao, Y. N. Liang, Y. Zhou and G. Zhao, *Carbohydr. Polym.*, 2019, **213**, 79–88.
26 S. Ahmadzadeh and A. Ubeyitogullari, *Carbohydr. Polym.*, 2023, **301**, 120296.
27 S. Dey, N. Hettiarachchy, A. A. Bisly, K. Luthra, G. G. Atungulu, A. Ubeyitogullari and L. A. Mozzoni, *J. Food Sci.*, 2022, **87**, 4808–4819.
28 A. Ubeyitogullari and O. N. Ciftci, *RSC Adv.*, 2016, **6**, 108319–108327.
29 Y. Sun, Z. Wu, B. Hu, W. Wang, H. Ye, Y. Sun, X. Wang and X. Zeng, *Carbohydr. Polym.*, 2014, **108**, 153–158.
30 T. Wang, J. D. Jones, I. I. Niyonshuti, S. Agrawal, R. K. Gundampati, T. K. S. Kumar, K. P. Quinn and J. Chen, *Adv. Ther.*, 2019, **2**, 1900092.
31 R. M. Saunders, *Cereal Foods World*, 1990, **35**, 632–636.
32 C. Fabian and Y.-H. Ju, *Crit. Rev. Food Sci. Nutr.*, 2011, **51**, 816–827.
33 A. Abdul-Hamid and Y. S. Luan, *Food Chem.*, 2000, **68**, 15–19.
34 B. S. Luh, in *Cereals Processing Technology*, Elsevier, 2001, pp. 79–108.
35 R. Vaitkeviciene, J. Bendoraitiene, R. Degutyte, M. Svazas and D. Zadeike, *Polymers*, 2022, **14**(17), 3662.
36 T. P. Singh and D. S. Sogi, *Starch – Stärke*, 2018, **70**, 1700242.
37 C. Fabian, A. Ayucitra, S. Ismadji and Y.-H. Ju, *J. Taiwan Inst. Chem. Eng.*, 2011, **42**, 86–91.
38 M. Alexandri, J. López-Gómez, A. Olszewska-Widdrat and J. Venus, *Fermentation*, 2020, **6**(2), 42.
39 C. Kalpanadevi, V. Singh and R. Subramanian, *J. Food Sci. Technol.*, 2018, **55**, 2259–2269.
40 A. Ubeyitogullari and O. N. Ciftci, *Food Hydrocolloids*, 2020, **102**, 105597.
41 M. Reis, M. Brito Sousa, F. Alobaid, C. Bertran and Y. Wang, *Adv. Powder Technol.*, 2018, **29**, 1571–1581.
42 R. M. Saunders, *Food Rev. Int.*, 1985, **1**, 465–495.
43 Y. Wang, M. He, Y. Wu, Y. Liu and J. Ouyang, *Starch - Stärke*, 2021, **73**, 2000161.
44 I. Selmer, C. Kleemann, U. Kulozik, S. Heinrich and I. Smirnova, *J. Supercrit. Fluids*, 2015, **106**, 42–49.
45 G. M. Glenn and D. W. Irving, *Cereal Chem.*, 1995, **72**, 155–161.
46 A. Rahman and T. Oomori, *J. Cryst. Growth*, 2008, **310**, 3528–3534.
47 L. Niu, L. Wu and J. Xiao, *Carbohydr. Polym.*, 2017, **175**, 311–319.
48 X. Lu, R. Ma, J. Zhan, Z. Jin and Y. Tian, *NPJ Sci. Food*, 2022, **6**, 37.
49 H. F. Zobel, *Starch – Stärke*, 1988, **40**, 1–7.
50 N. Abhari, A. Madadlou and A. Dini, *Food Chem.*, 2017, **221**, 147–152.
51 A. Ubeyitogullari and O. N. Ciftci, *Carbohydr. Polym.*, 2016, **147**, 125–132.
52 D. Muscat, R. Adhikari, M. J. Tobin, S. McKnight, L. Wakeling and B. Adhikari, *Carbohydr. Polym.*, 2014, **111**, 333–347.
53 A. Ubeyitogullari, S. Brahma, D. J. Rose and O. N. Ciftci, *J. Agric. Food Chem.*, 2018, **66**, 9490–9497.
54 E. Pereira, S. Einloft, M. Seferin, L. M. dos Santos, J. Lima and R. Ligabue, *Waste Biomass Valorization*, 2019, **10**, 755–762.
55 E. Hasanvand and A. Rafe, *Food Biophys.*, 2018, **13**, 387–395.
56 N. J. Babu and A. Nangia, *Cryst. Growth Des.*, 2011, **11**, 2662–2679.
57 S. Bhosale and D. Vijayalakshmi, *Curr. Res. Nutr. Food Sci. J*, 2015, **3**, 74–80.
58 V. Singh, H. Okadome, H. Toyoshima, S. Isobe and K. I. Ohtsubo, *J. Agric. Food Chem.*, 2000, **48**, 2639–2647.
59 S. Tang, N. S. Hettiarachchy, R. Horax and S. Eswaranandam, *J. Food Sci.*, 2003, **68**, 152–157.